Molecular Dynamics Simulation of Bovine Prothrombin Fragment 1 in the Presence of Calcium Ions†

Nobuko Hamaguchi,‡ Paul Charifson,§,‖ Tom Darden,⊥ Lynn Xiao,# Kaillathe Padmanabhan,▽ Alexander Tulinsky,▽ Richard Hiskey,# and Lee Pedersen*,⊥,#

Department of Biology, University of North Carolina, Chapel Hill, North Carolina 27599, Cray Research, Inc., P.O. Box 12746, Research Triangle Park, North Carolina 27709, National Institute of Environmental Health Sciences, Research Triangle Park, North Carolina 27709, Department of Chemistry, University of North Carolina, Chapel Hill, North Carolina 27599, and Department of Chemistry, Michigan State University, East Lansing, Michigan 48824

Received April 22, 1992; Revised Manuscript Received July 2, 1992

ABSTRACT: Early solvation-induced structural reorganization of calcium prothrombin fragment 1 is simulated with molecular dynamics. Initial coordinates are those of the 2.2-Å resolution crystal structure [Soriano-Garcia, M., Padmanabhan, K., de Vos, A. M., & Tulinsky, A. (1992) *Biochemistry 31*, 2554–2556]. The molecular dynamics code AMBER, appropriately modified to include long-range (≤22.0 Å) ionic forces, was employed. The solution structure appears to equilibrate within 100 ps. Although minor changes are seen in various structural domains, the early solution structure basically maintains an intricate network of nine γ-carboxyglutamic acid (Gla) residues encapsulating seven calcium ions. However, the Gla domain moves with respect to the kringle domain. This motion is mainly due to the movement of Ser34–Leu35 that appears to be a flexible hinge between the domains. The N-terminus of Ala1 is in a tightly bound complex with three Gla residues that remains stable in the solution structure when the long-range electrostatic cutoff is employed and the near planar alignment of the seven calcium ions is only slightly distorted. The simulation structure is discussed in terms of experiments that studied calcium ion-induced quenching of the intrinsic fluorescence, protection of the N-terminal amino group from acetylation by calcium ions, chemical modification of the N-terminus to a trinitrophenyl derivative, and the possibility of a calcium-binding site(s) in the kringle domain.

Prothrombin, one of several vitamin-K dependent proteins involved in the blood coagulation cascade, is converted to thrombin by the prothrombinase complex on the surface of membranes (Suttie & Jackson, 1977). Thrombin subsequently catalyzes the conversion of fibrinogen to fibrin that forms the essential fibrin clot. Thrombin also plays an important physiological role in the enhancement, attenuation, and regulation of other haemostatic processes (Mann, 1987).

Fragment 1 of bovine prothrombin is the 1–156 N-terminal peptide of the protein (Figure 1) that can bind to membrane. Ten glutamic acid residues within the first 33 residues of the N-terminus region are normally posttranslationally modified by a vitamin-K dependent carboxylase to Gla[1] (Suttie, 1988; Olson, 1984). It appears certain that the Gla residues are responsible, at least in part, for the membrane binding of prothrombin and other members of this family, which includes proteins C, S, and Z and factors VII, IX, and X. Studies of fluorescence (Nelsestuen, 1976; Pendergast & Mann, 1977), circular dichroism (Bloom & Mann, 1978), and equilibrium dialysis (Deerfield et al., 1987) have indicated that a number of different metal ions will bind to the Gla domain of bovine fragment 1. The calcium ion binding is a cooperative process (Deerfield et al., 1987) and binding of fragment 1 to a membrane surface requires the presence of calcium ions. Taken together, the indirect experimental evidence has suggested that the initial cooperative calcium ion binding causes a conformational change, with the binding of additional calcium

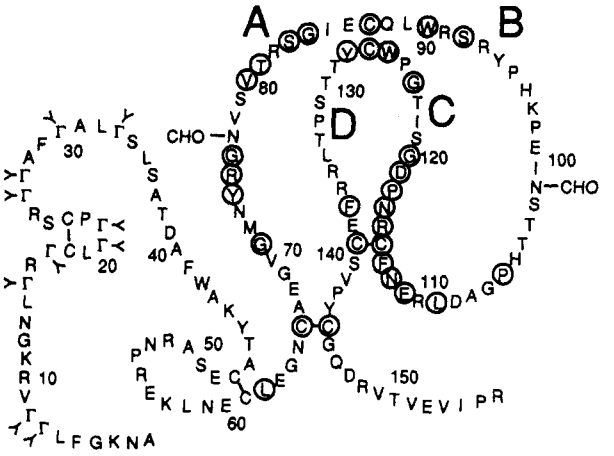

FIGURE 1: Sequence of bovine prothrombin fragment 1. Γ, γ-carboxyglutamic acid, Gla: circled residues are conserved with kringle 2 of prothrombin; CHO, biantennary carbohydrate chains.

† This work was supported in part by grants from the NIH Heart, Lung, and Blood Institute, Grant numbers HL-27995, HL-20161, HL-25942, HL-43229, and HL-06350.

* Author to whom correspondence should be addressed.
‡ Department of Biology, University of North Carolina, Chapel Hill.
§ Cray Research, Inc.
‖ Current address: Glaxo, Inc., 5 Moore Dr., Research Triangle Park, NC 27709.
⊥ National Institute of Environmental Health Sciences.
Department of Chemistry, University of North Carolina, Chapel Hill.
▽ Michigan State University.

[1] Abbreviations: Ace-Ala1/bf1, *N*-acetyl-bf1, apo-bf1, the crystal structure of bovine prothrombin fragment 1 (residues 36–156); avg-bf1/Ca, the average simulation structure (97–116 ps) of bovine prothrombin fragment 1 (1–145); bf1, bovine fragment 1 (residues 1–145); bf1/Ca, the crystal structure of bovine prothrombin fragment 1 (residues 1–145) in the presence of calcium ions; Gla, γ-carboxyglutamic acid; Gla domain, fragment 1 (residues 1–34), previously designated (residues 1–48) (Soriano-Garcia et al., 1989, 1992); kringle domain, fragment 1 (residues 66–145); TNP-Ala1/bf1, *N*-trinitrophenyl-bf1; rmsd, root mean square deviation; when minimizing or reminimizing is mentioned, it refers to the energy.

0006-2960/92/0431-8840$03.00/0

ions serving to bridge the Gla domain carboxylate side chains to the phosphate head groups of the membrane surface. An involvement of the kringle domain in membrane binding has also been implicated by recent chemical modification studies (Welsch & Nelsestuen, 1988b; Weber et al., 1992). A weak calcium ion binding site in the kringle domain has been inferred by a hydrophobic column technique (Lundblad, 1988) and by equilibrium dialysis studies employing an isolated kringle domain (Berkowitz et al., 1992). However, a detailed mechanism for the calcium-mediated binding of prothrombin fragment 1 to membrane surfaces has not been yet fully described.

Residues 1–36 of apo-bf1, as well as the carbohydrate side chains of Asn77 and Asn101, have been shown to be crystallographically disordered in the absence of calcium ions (Park & Tulinsky, 1986; Tulinsky et al., 1988; Seshadri et al., 1991). Recently, the structure of bf1/Ca was determined in the presence of 100 mM $CaCl_2$ (Soriano-Garcia et al., 1992), where carbohydrate remains disordered but the Gla domain has an ordered structure and interacts with seven calcium ions. A spectacular feature of this structure is the manner in which nine of the ten Gla residues are clustered around the seven calcium ions in an intricate network heretofore unobserved in biological systems.

Molecular dynamics provides a very useful technique to estimate the changes that occur when a protein is solvated. Moreover, the development of a theoretical methodology to properly describe macromolecular systems of substantial charge possessing multiple metal–protein interactions is of more than passing interest and importance. The bf1/Ca system is uniquely suited for this purpose to serve as a model to follow the evolution of the early solvated structure of a highly charged system with numerous well-defined ions. We report here the results of a 116-ps molecular dynamics simulation of the solution structure of bf1/Ca. The structure equilibrates in approximately 80 ps and displays a motion of the Gla domain relative to the kringle with the respective domains essentially maintaining their crystallographic structures including the seven calcium ions. Such domain motions could be of significant functional consequence in haemostasis and fibrinolysis where multidomain protein structures are a common occurrence.

MATERIALS AND METHODS

AMBER version 3A (Weiner et al., 1984, 1986) was used for the molecular dynamics simulations based on the coordinates of bf1/Ca (Soriano-Garcia et al., 1992). This bf1/Ca structure only extended to the last cysteine of the kringle domain; part of the interbridge peptide (146–156) appears to be removed during crystallization, and the remaining residues are disordered in the crystal structure (Olsson et al, 1982; Soriano-Garcia et al., 1989, 1992). The simulations utilized the all-atom force field (Weiner et al., 1986) with a single nonbonded cutoff of 10.0 Å for energy minimization and a twin cutoff, which is discussed below, for molecular dynamics. The molecules were immersed in a box of TIP3P water (Jorgensen et al., 1983); approximately 8500 water molecules solvated bf1/Ca. All covalent bonds involving hydrogens were constrained, and 3 amu was used for all hydrogens. The simulations were performed at 300 K (after initial step-wise heating over the first 3 ps of the simulation), the integration step size was 1 fs, and the nonbonded list was updated every 20 steps. At each interval the nonbonded list was updated and the forces were corrected to include the effect of electrostatic and attractive van der Waals interactions in the range between 10.0 and 22.0 Å. The inclusion of this long-range force correction, which had been suggested by Berendsen et al. (1986), proved to be essential for stabilizing the structure over a long simulation, particularly in the region of Ala1. A test simulation performed using a 10.0-Å cutoff without the long-range correction developed an instability in this region, and ultimately Ala1 detached from a well-defined pocket in which it is highly interactive with three Gla residues in the crystal structure (Soriano-Garcia et al., 1992).

Appropriate code modifications were made to ensure that the protein and water bath did not have diverging temperatures. The partial charges and parameters for calcium ions and Gla residues were taken from Charifson et al. (1991) and Maynard et al. (1988). The computations were carried out on CRAY Y-MP supercomputers at the North Carolina Supercomputing Center (Research Triangle Park, NC) and at the National Cancer Institute (Frederick, MD). Essential graphics were performed on an IRIS-VGX workstation using the program MULTI (Darden et al., 1991).

Several modifications were made to AMBER to increase the throughput. The SHAKE algorithm was modified to conform to the modified Newton method suggested by Ryckaert et al. (1977). This algorithm replaces the normal AMBER interative SHAKE procedure by a linearization of the simultaneous quadratic equations. SHAKE is known to be slowly convergent on cyclic structures, such as TIP3P water, whereas the modified Newton method converges rapidly. A speedup of approximately 20% results. Computation of the nonbonded list was modified by implementation of a grid technique. The size of the grid was determined by one-half the nonbonded cutoff; interactions greater than two grid units apart are not tested. This innovation resulted in another speedup of approximately 20% for the problem. The manner in which the solvent–any atom interactions are computed was modified by preprocessing the nonbonded list of the solvent–any atom interactions, using to advantage the fact that the hydrogen atoms of the rigid TIP3P water molecules are assigned no van der Waals interactions. This implementation, along with preimaging the water molecules that have a high probability of being imaged (those within one nonbonded cutoff of the box side), led to a substantial speedup of approximately 40%. Finally, the box was recentered to the center of the protein coordinates at every step; this led to an improvement in the efficiency of the computation by avoiding minimum image conflicts. The net increase in speed as the result of these improvements in the code was nearly a factor of 2. Approximately 1 ps of simulation time per 2–3 cpu hours were obtained on a single CRAY Y-MP processing element. A parallel version of the code which ulitized multiple processors was also constructed.

The simulations were prepared and conducted according to the following protocol. All covalently bonded hydrogen atoms were added to bf1/Ca and minimized (without explicit solvent) while keeping the protein heavy atoms fixed. The crystallographic R value for this structure plus the crystallographically determined water molecules was 0.180, which compares well with the final $R = 0.171$ of the crystallographic refinement (Soriano-Garcia et al., 1992). Hydrogen atoms were added to the crystallographically determined water oxygen atoms and minimized using a distance-dependent dielectric function ($\epsilon = r$). Then, 20 ps of molecular dynamics simulation was performed keeping the oxygen positions of the water molecules and all protein atoms fixed. Reminimization of the water hydrogen atoms was then performed. Solvation was accomplished by defining a box of water with each side being at least

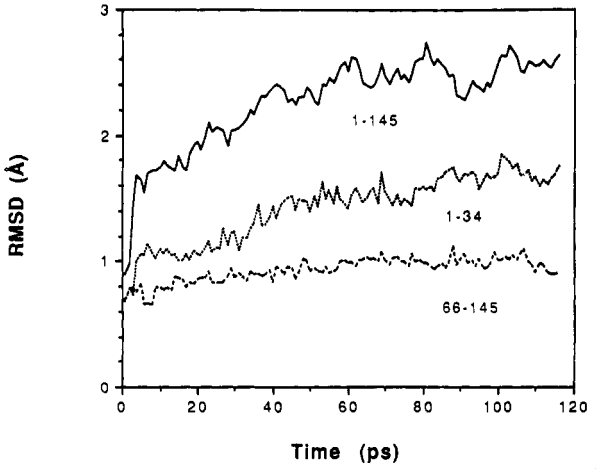

FIGURE 2: Root mean square deviations of the backbone atoms of the simulation structure from those of the whole structure (solid line), kringle domain (coarse dotted line), and the Gla domain (fine dotted line).

13 Å from the nearest protein atom. The water molecules were placed so as to have no oxygen atom closer than 2.8 Å or water hydrogen atom closer than 2.0 Å to any protein atom. The large box of water was minimized at constant volume while holding the protein atoms stationary. Twenty picoseconds of dynamics was subsequently performed on the water only. The water was then reminimized (holding the protein fixed) followed by a minimization of all atoms. The system was now considered ready for all-atoms dynamics. All computation in the water box were carried out with $\epsilon = 1.0$.

In any theoretical treatment it is important to indicate some of the major assumptions and approximations underlying the calculations. One is that the force field model is simplistic in that terms involving mixed motion, sometimes called cross terms, are not included. The charge distribution for the protein, ions, and water is static; dynamic polarization and charge exchange are not included. The TIP3P model for water is a simple rigid three-point model and does not permit distortion. Newton's equations are solved using numerical integration and, given approximately 116 000 steps, the solution is subject to numerical limitations and some degree of fluctuation. Although counterions, such as chloride ions, as well as bulk, unbound calcium ions, were undoubtedly present in the solvent surrounding the protein molecules in the crystal, the only ones in the simulation were the seven calcium ions bound to the protein. Even with the large (22.0-Å) cutoff for the nonbonded electrostatic and attractive van der Waals interactions, spurious behavior will ultimately result in a very long simulation. Notwithstanding such an array of obstacles, the molecular dynamics simulation was both well-behaved throughout and reasonable in predicting the motion of a structural domain relative to another one.

RESULTS AND DISCUSSION

Global Aspects of the Simulation Structure. The molecular dynamics simulation was carried out for 116 ps using the protocol discussed under Materials and Methods. A decision to terminate the simulation was based on the apparent equilibration of the rmsd of the backbone atoms. The rmsd was computed by comparing the structure at any given time with the crystal structure (Soriano-Garcia et al., 1992). The time dependence of the rmsd of the Gla domain, the kringle domain, and the entire structure is shown in Figure 2. Clearly, all three groups have reached pseudoequilibration by 116 ps. An average structure was calculated from the atomic coordinates of the final 20 ps (97–116 ps); the average rmsd of avg-bfl/Ca and its domains from bfl/Ca is given in Table I. The avg-bfl/Ca structure was compared to the ideal structure used in the crystallographic refinement; the statistics are given in Table II. A comparison of the backbone structure of bfl/Ca with that of avg-bfl/Ca is shown in Figure 3. Either the kringle (Figure 3a) or the Gla domain (Figure 3b) in avg-bfl/Ca is superimposed with the respective domain from bfl/Ca. From Figure 3a,c, it can be seen that *the two domains move with respect to one another* and, from Figure 3a,b, that the kringle domain shows a smaller internal deviation than the Gla domain. Since the Gla and the kringle domains approximate discoids in the crystal structure (Figure 3c), the relative motions of the domains can be described simply by calculating an average plane for each domain and determining the angles between these planes. The results are shown in Table III, which includes apo-bfl (Seshadri et al., 1991), bfl/Ca, and avg-bfl/Ca. The largest change is between the Gla domain and the kringle domain of bfl/Ca and avg-bfl/Ca (42°). This interdomain motion is clearly seen in Figure 3a,c.

This motion between domains is mainly due to the backbone motion at Ser34 and Leu35, which appears to provide an additional hinge responsible for the flexibility between domains in the simulation. A previously suggested hinge region (Leu62–Asn65) was inferred by comparing crystal structures with and without calcium. However, it was found to be relatively stable compared to the Ser34–Leu35 hinge during the solution simulation.

Table I: Root Mean Square Deviations (Å) of Domains of bfl/Cα[a]

	residue units			
atoms	Gla domain 1–34	helix–loop 35–65	kringle 66–145	bfl/Ca 1–145
N, CA, C	1.7	1.0	0.9	2.52
all atoms	2.3	1.8	1.3	2.82

[a] The comparison is between the crystal structure and the average simulation structure (97–116 ps).

Table II: Summary of Root Mean Square Deviations of avg-bfl/Ca from Ideal Structure of Crystallographic Refinement

distances (Å)	rmsd	nonbonded contacts (Å)	rmsd
bond lengths	0.043	single torsion	0.17
bond angles	0.071	multiple torsion	0.23
planar 1–4	0.073	possible H-bond	0.11
planes (Å)		torsion angles (deg)	
peptides	0.045	planar	8.5
aromatic groups	0.035	staggered	17
		orthonormal	33
chiral volumes (Å^3)	0.16		

Table III: Angles between the Planes of Structural Domains of Apo- and Calcium Fragment 1[a]

domains	apo-bfl (deg)	bfl/Ca (deg)	avg-bfl/Ca (deg)
helix (36–47) vs loop–kringle (48–145)	21[b]	53	42
Gla (1–34) vs connecting (35–65)		57	67
connecting (35–65) vs kringle (66–145)	47[b]	57	51
Gla (1–34) vs kringle (66–145)		27	69

[a] Average planes of the Cα's were employed. [b] In apo-bfl, residues 36–65 and 66–156 were used to calculate the best fit planes between the connecting region and kringle domain, respectively. The helix pivots by 30° in forming bfl/Ca from apo-bfl (Soriano-Garcia et al., 1992).

Table IV: Intermolecular Crystal Contacts That Are Lost upon Solvation in Solution[a]

molecule 1	molecule 2	distance (Å)	type of interaction[b]
CE2-Phe5	OG-Ser36	3.7	vdW
CE2-Phe5	CA-Ala37	3.1	np-vdW
CZ-Phe5	CB-Ala40	3.4	np-vdW
CD1-Leu6	O-Ala37	3.3	vdW
CD2-Leu6	C-Ala40	3.9	np-vdW
O-Gla8	OE2-Gla15	3.1	charged-vdW
O-Gla8	CD1-Leu19	3.5	vdW
CG1-Val9	CD1-Leu62	3.8	np-vdW
CG2-Val9	CE1-Phe41	3.8	np-vdW
OE1-Gla15	Ca-2	3.7	ionic
OE1-Gla30	Ca-7	4.3	ionic
OG-Ser50	CG-Pro132	3.9	vdW
CB-Ala67	CE1-Tyr94	3.6	np-vdW
OE1-Glu68	CB-Pro132	3.6	vdW
O-Gly69	CB-Tyr94	3.3	vdW
O-Gly69	CA-Pro95	3.7	vdW
NH1-Arg82	CD-Arg93	2.4	charged-vdW
CD2-Leu89	CD2-Ile122	2.7	np-vdW
O-Arg91	OE2-Glu 138	3.8	charged-vdW
OB-Ser92	CG2-Thr123	3.9	vdW
OG-Ser92	O-Ile122	3.6	p-vdW
N-Arg93	OE1-Glu138	3.5	charged-vdW
CZ-Arg93	CB-Ser140	3.9	np-vdW
NH1-Arg93	O-Val141	3.3	charged-vdW
O-Tyr94	O-Ile122	3.5	p-vdW
CD2-Tyr94	O-Thr123	3.2	vdW
CE2-Tyr94	CA-Gly124	3.8	np-vdW
CZ-Tyr94	CD-Pro125	3.6	np-vdW
OH-Tyr94	O-Cys139	2.5	hydrogen bond
OH-Tyr94	N-Val140	3.0	hydrogen bond
O-Pro95	CG1-Val143	3.7	vdW
Ca-1	Ca-7	(4.7)	

[a] Only the shortest contact between two residues (less than 4.0 Å) is listed. [b] np-vdW, homonulcear van der Waals interaction; vdW, heteronuclear van der Waals interaction; charged-vdW, one atom charged in van der Waals interaction.

Intermolecular Contacts Lost with Solvation. There are two major considerations influencing structural elements that move in bf1/Ca during such a solvation simulation. One is general and corresponds to the intermolecular crystal contacts that are lost; the other is special to bf1/Ca and applies to the carbohydrate moieties attached to Asn77 and Asn101. The carbohydrate chains are disordered in bf1/Ca (Soriano-Garcia et al., 1992) so that the simulation structure does not account for them (simple Asn groups at positions 77 and 101 are assumed). The side chains of Asn77 and Asn101 form hydrogen bonds in the simulation to the side chain of Arg116 and the backbone nitrogen of Ser102, respectively, but no significant distortion of backbone positions of these residues was observed. The intermolecular contacts <4.0 Å for the crystal structure are listed in Table IV. These contacts are replaced by water or intramolecular interactions upon solvation. Since the unit cell is approximately 60% solvent, it might be expected that most of the intermolecular contacts would involve side chains, and the data in Table IV show that this is the case. The backbone atoms of Gla8 interact with the side chain of Gla15 in a symmetry-related molecule, and the side chain of Gla15 interacts weakly (3.7 Å) with Ca-2 that is bound in a symmetry-related molecule. No calcium in any molecule is within 4.5 Å of a calcium of another molecule.

A comparison of the variance, $\langle (x - \langle x \rangle)^2 \rangle$, of avg-bf1/Ca over the final 20 ps and the crystallographic B factors ($8\pi\mu^2$) of bf1/Ca (mean square isotropic displacements proportional to the variance of the crystallographic structure) is shown in Figure 4 from which it can be seen that regions of smaller variance in bf1/Ca are associated with intermolecular crystal contacts, which surprisingly do not increase in general in the solution simulation. Moreover, the tetradecapeptide 48–61 disulfide loop, about half of the second outer B loop of the kringle (96–108) (Figure 1), and the C-terminal 136–145 segment of the kringle appear to be considerably more flexible in the crystal structure, suggesting positional disorder in the latter. The 96–108 region, where carbohydrate is attached to Asn101, also showed a large movement on binding calcium ion to apo-bf1 (Soriano-Garcia et al., 1992). However, the average variances of bf1/Ca (0.36 Å^2) and avg-bf1/Ca (0.27 Å^2) are very comparable.

The larger variance in avg-bf1/Ca between Ser34 and Ser36 corresponds to the new hinge region developed in the solution simulation, while the large anomaly at Arg10–Gly12 is due to the arginyl side chain extending into solvent adjacent to Lys11, which is disordered in bf1/Ca. In the crystal, Arg10 and Arg16 appear to form a complex ion pair with a nearby chloride or cacodylate counterion (Soriano-Garcia et al., 1992). Only the variance of avg-bf1/Ca between Gly120 and Gly124 corresponds to a large increase in flexibility due to the loss of intermolecular crystal contacts. It is notable that this region also happens to correspond to the cationic binding center in lysine/fibrin binding kringles (Mulichak et al., 1991; Wu et al., 1991) so that the solution flexibility might reflect functional significance.

Comparison of Intramolecular Domain Interactions. The only important intramolecular domain–domain interactions essentially occur between the Gla domain and the Cys48–Cys61 disulfide loop, and they are compared in Table V for bf1/Ca and avg-bf1/Ca (contacts less than 5.0 Å). The average interdomain interaction distance is about 0.5 Å longer in avg-bf1/Ca. This is directly related to the pivot of the Gla domain with respect to the Ser34–Leu35 hinge. These two domains are more closely associated in bf1/Ca where, in tandem, they resemble an independent structural domain (Soriano-Garcia et al., 1992).

Interactions which are lost or weakened upon solvating bf1/Ca are those between Lys44–Leu62, Ser50–Glu68, Arg52–Cys18, and Gla21, and Arg55–Leu19 and Gla20. The remaining interactions are essentially unchanged but include some rotation of side chains, especially near the surface when not involved in stabilizing interactions. The side groups tend to extend out into solvent in such cases giving an overall swelling impression to the solution structure. A strong ion pair interaction is firmly maintained during the simulation between Gla15 and Arg55, and a new one is generated between Lys57 and Glu68; the latter interaction bridges the kringle and its preceding disulfide loop as does the one between Cys61 and Asn73. However, one ion pair is lost (Arg25–Asp39), and one (Arg55–Gla20) is diminished in the simulation along with the loss of five hydrogen bonds (Table V).

The crystallographic structure has two interdomain contacts between the Gla domain and the connecting helix: Cys23–Tyr45 (backbone–side chain) and Arg25–Asp39 (side chain–side chain). Both contacts lost in the simulation structure are replaced by longer interactions between Leu19 and Tyr45 (backbone–side chain) and Arg25 and Trp42 (side chain–side chain). These changes indicate that the Gla domain and the connecting helix have also moved apart somewhat during the solvation process.

The Calcium Network. A remarkable aspect of the positions of the calcium ions in the crystal structure is their close juxtaposition to one another (between 4 and 6 Å). Even more remarkable is that this network is essentially maintained over 116 ps of simulation (Figure 3b), attesting to the stability of

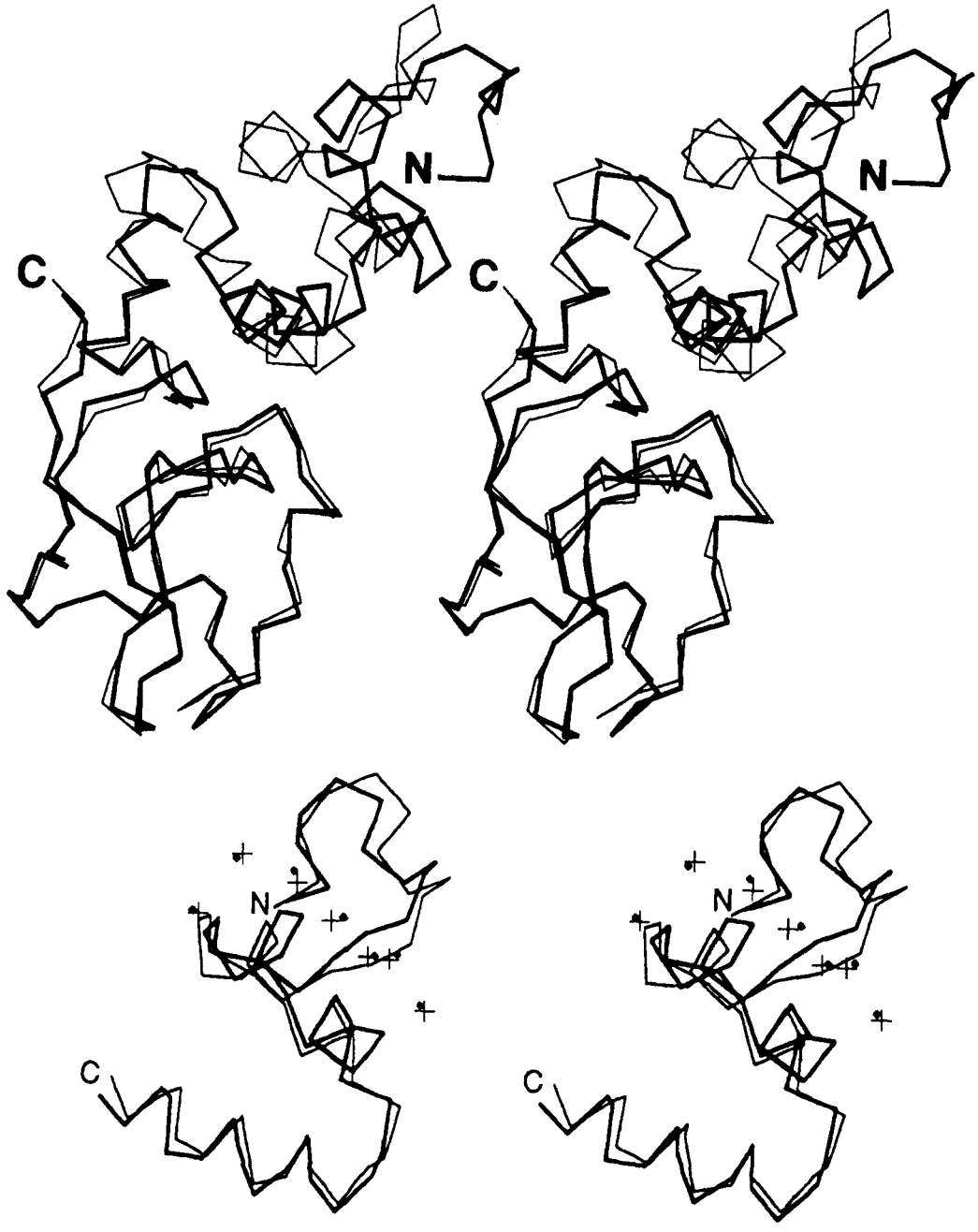

its makeup. The distances between calcium ions in bf1/Ca and in avg-bf1/Ca are summarized in Table VI. Both structures have six calcium–calcium distances less than 5.4 Å. The average deviation between crystal and simulation for all 21 unique distances is only 0.58 Å; the largest deviation is 1.5 Å between Ca-4 and Ca-5 (Table VI). It is somewhat surprising that Ca-1 and Ca-7 do not show greater deviations since the intermolecular crystal contact between these two calciums ions is 4.7 Å and they have smaller coordination numbers of four and three, respectively (Soriano-Garcia et al., 1992). All other intermolecular calcium–calcium distances are greater than 5.5 Å.

In Figure 5a, the best fit of the positions of the seven calcium ions (crystal vs simulation) shows that Ca-5 has been displaced to the greatest extent. The thermal motion parameters of the calcium ions are shown in Figure 5b, which compares them with the variances of the ions over the final 20 ps of simulation. Although the variance is about 1.5 greater than the isotropic mean square displacement of the *B* factors, the coincidence of the relative motions of calcium ions 2–7 is striking, with Ca-5 showing the largest motion. The position of Ca-1 clearly has a much greater variance in the solution structure that is most likely the result of the loss of the intermolecular crystal contact that produces an infinite chain of calcium ions in the crystal (Soriano-Garcia et al., 1992).

The small calcium–calcium distances observed in bf1/Ca have also been observed in other systems. The calcium structure of thermolysin has four calcium sites, two of which are within 3.8 Å of each other (Holmes & Matthews, 1982). An interesting feature of the calcium network in bf1/Ca is the near-planar arrangement of the calcium ions. The average deviation from the best plane is 0.32 Å for the crystal structure and 0.59 Å for the solution structure (Table VII); Ca-3 is essentially the only ion displaced out of the plane in the crystal structure, while Ca-1 is also displaced in avg-bf1/Ca. In addition, the calcium ions of both structures fall on the same relative side of the plane. The one exception is Ca-6, which is in the calcium plane in the crystal structure and is about 0.7 Å off the plane in the solution structure.

FIGURE 3: Comparisons of the Cα structure of bf1/Ca and avg-bf1/Ca. (a, opposite page, top) Stereoview of superposition of kringle domains; avg-bf1/Ca is shown in bold, X-ray in light trace; Ala1 and Cys145 are indicated with N and C, respectively; disulfide bonds are not shown. (b, opposite page, bottom) Stereoview of the superposition of Gla domains only; avg-bf1/Ca's in bold; Ala1 and Cys48 are indicated with N and C, respectively; disulfide bonds are not shown; calcium ions are shown as squares in bf1/Ca and as crosses in avg-bf1/Ca. (c, above) Monoview comparing bf1/Ca (left) and avg-bf1/Ca (right); the view is 90° from that in (a).

Table V: Comparison of Interdomain Interactions of bf1/Ca and avg-bf1/Ca Structures

interaction		bf1/Ca (Å)	avg-bf1/Ca (Å)
Cys23 N	Tyr45 OH	2.8 H-bond	6.7
Arg25 NH1	Asp39 OD2	2.2 ion pair	7.7
Leu19 O	Tyr45 OH	8.1	3.4
Arg25 NH1	Trp42 NE1	6.6	3.4
Lys44 NZ	Leu62 O	2.7 H-bond	4.3
Ser50 OG	Glu68 OE1	3.0 H-bond	4.3
Ala51 N	Glu68 OE1	4.9	3.8
Arg52 NH1	Gla20 O	6.6	4.7 ion pair
	Cys18 O	3.1 H-bond	6.9
	Gla21 O	3.2	4.4
Arg55 NH1	Gla15 OE1	6.0	2.4 ion pair
	OE3	2.2 ion pair	3.7 ion pair
Arg55 NH2	OE3	3.4 ion pair	2.7 ion pair
	OE4	3.3 ion pair	4.7 ion pair
	Leu19 O	2.5 H-bond	5.3
	Gla20 OE4	2.9 ion pair	4.7
Lys57 NZ	Glu68 OE2	5.9	2.7 ion pair
Glu60 OE2	Gly145 N	3.1 H-bond	9.8
Cys61 O	Asn73 ND2	2.9 H-bond	2.8 H-bond

The Calcium–Gla Network. The coordination of the calcium ions by the carboxylate groups of the Gla residues of the solution structure is compared with that of bf1/Ca in Table VIII. Examination of Table VIII shows (a) Ca-1, -2, -3, -4, and -6 have identical Gla coordinations in both structures; (b) Ca-5 shows the greatest change in Gla coordination, losing two ligands but gaining one in going to avg-bf1/Ca, which is consistent with the large change generally associated with Ca-5 (Figure 5a); (c) Gla15 and Gla26 interact with only one calcium ion, Ca-7 and Ca-1, respectively; (d) all calcium ions interact with at least two Gla residues; Ca-3 and 4 interact with four Gla residues; (e) the paucity of water coordination to the calcium ions observed in bf1/Ca (Soriano-Garcia et al., 1992) is maintained in solution, with only five molecules of water coordinated to calcium in bf1/Ca and seven in avg-bf1/Ca; (f) calcium ions 1, 6, and 7 have the greatest number of open coordination positions and so might be expected to be the most likely to interact with another molecule in self-association or with a negatively charged phospholipid surface in membrane binding; (g) Gla33 is disordered in bf1/Ca, and, although included in the simulation, no coordination with calcium developed over the course of the simulation.

Table VI: Inter-Calcium Ion Distances (Å) for bf1/Ca (Upper Half of Matrix) and for avg-bf1/Ca (Lower Half of Matrix)

		1	2	3	4	5	6	7
	1		4.4	7.1	9.5	13.4	18.4	22.6
	2	4.1		4.0	5.3	9.1	14.3	19.4
	3	6.8	4.0		3.8	7.1	11.7	15.8
avg-bf1/Ca	4	8.6	4.8	3.8		3.8	9.0	14.7
	5	13.9	10.1	8.1	5.3		5.3	12.3
	6	17.9	14.3	12.0	9.5	4.5		8.5
	7	21.7	18.9	15.5	14.7	10.9	7.6	

The crystals used to determine the structure of bf1/Ca were grown from a 100 mM $CaCl_2$ solution. Thus, the effective concentration of bound calcium within crystals is about 130 mM, so that there are many chloride ions in the crystal. These are not accounted for in the simulation since they were not required to balance charge. The physiological concentration

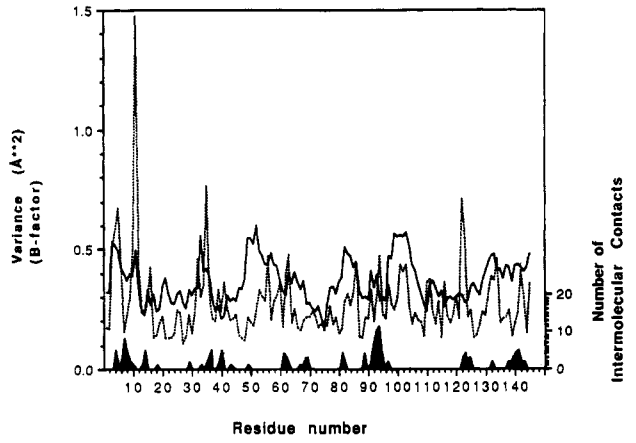

FIGURE 4: Comparison of the variance in the simulation with crystallographic *B* factors or mean square isotropic displacements (μ^2). *B* factors, solid line; solution variance, dotted line; number of intermolecular contacts, shaded along abcissa. Variances and *B* factors are the average of each residue. Atoms not included in crystallographic refinement for lack of electron density (side chains Lys3, Lys11, Gla33) are assigned $B = 50$ Å^2.

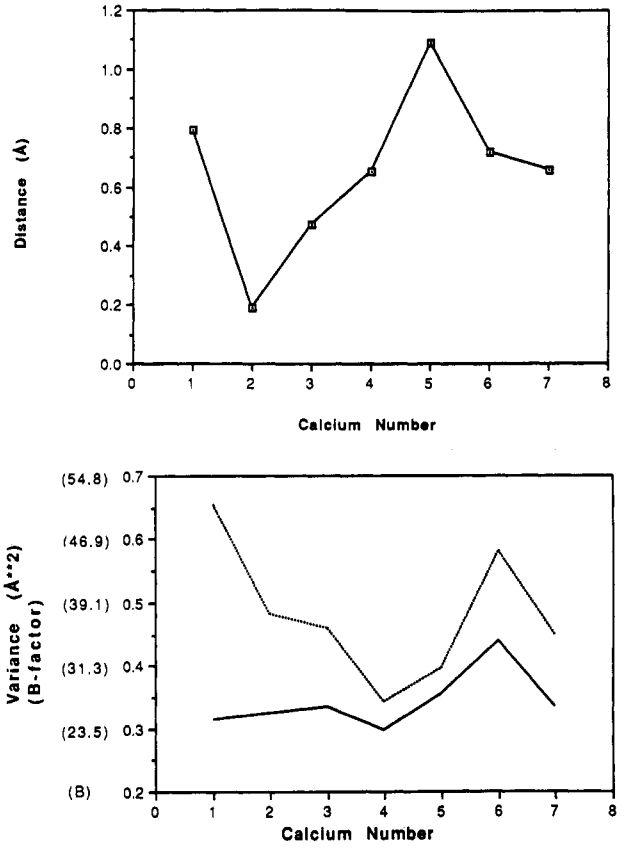

FIGURE 5: Calcium ion structure. (a, top) Deviation of calcium positions between crystal and the average simulation structure based on fit of calcium position only. (b, bottom) Crystallographic *B* factor (solid line) and variance of average solution structure (dotted line) for calcium ions.

of calcium ion (2 mM) is sufficient for the conformational change required for function. Ca-2, -3, -4, and possibly Ca-5 are likely the high affinity cooperative calcium-binding sites (Deerfield et al., 1987) expected to be occupied at this calcium concentration. The other calcium-binding sites might or might not be the result of the higher calcium concentration in crystals.

The Ala1 Interaction. A notable feature of bf1/Ca is the complex interaction of the amino group of the N-terminus with other groups of the Gla domain (Soriano-Garcia et al., 1992). The N-terminus is closely surrounded by carboxylate

Table VII: Distances of the Calcium Ions from the Best Plane Defined by the Seven Calcium Ions in bf1/Ca and avg-bf1/Ca[a]

	bf1/Ca	avg-bf1/Ca
Ca-1	−0.51	−1.14
Ca-2	−0.06	0.09
Ca-3	1.08	1.47
Ca-4	−0.33	−0.08
Ca-5	0.03	0.51
Ca-6	0.02	−0.68
Ca-7	−0.22	−0.18
av deviation	0.32	0.59

[a] Distances are in angstroms.

oxygen atoms from Gla residues at positions 17, 21, and 27 forming hydrogen-bonded ion pair interactions (Table IX); in addition, Ca-5 is within 2.8 Å while Ca-4 is only 3.7 Å away. The orientation is such that three Gla carboxylate oxygen atoms and the two calcium ions form a hemispheric array about N(1) (Figure 6) [torsion angles of C(1)–Cα-(1)–N(1)–X span approximately 180°]. The solution structure is generally similar to bf1/Ca at Ala1 with the exception that now a carboxylate oxygen from Gla7 is also nearby within hydrogen bonding and/or ion pair formation (2.8 Å) but at the expense of Ca-5 moving farther away from N(1) to a distance of 3.5 Å (Table IX; Figure 6). As in bf1/Ca, the torsion angles of the complexing groups span about 180°, except that there is a slight rotation of the complexing unit of the solution structure by approximately 30° as compared with bf1/Ca. The molecular dynamics simulation of bf1/Ca shows that the network involving the N-terminus applies to the solution structure as well as suggests that this unusual interaction between the α-amino group of Ala1, Gla residues, and calcium ions may be a new form of complexation among charged organic amines.

Effects of two different chemical modifications of the N-terminus of bf1 have been studied by Welsch and Nelsestuen (1988a) and Weber et al. (1992). These were N-acetylation and N-trinitrophenylation of the amino group at Ala1. The results of these studies show (1) calcium ions, but not magnesium ions, protected the N-terminus from acetylation by acetic anhydride and (2) both Ace-Ala1/bf1 and TNP-Ala1/bf1 can bind calcium, but only TNP-Ala1/bf1 retains membrane-binding capability. Since magnesium does not ligate to carboxylate oxygen atoms in a bidentate fashion, it is possible that some calcium-binding sites that have bidentate ligations (Ca-2, -3, -5, and -7; Table VIII) are highly calcium ion specific. The closest calcium to the amino group of Ala1 is Ca-5, which together with Ca-4, along with the three ion pair interactions involving Gla17, Gla21, and Gla27, may play a important role in the protection of Ala1 against the acetylation.

To predict the structural effects of these modifications, the models of bf1/Ca with either a TNP or an acetyl group at Ala1 were constructed. These groups were docked onto bf1/Ca so as to avoid steric conflicts as much as possible using the SYBYL software (Tripos Assoc., St. Louis, MO). The AMBER software was then employed to add hydrogens not present in the crystal coordinate file and to add a solution layer of 4.0 Å in thickness around the protein. An energy minimization of the entire structure and a preliminary molecular dynamics simulation on each system of 54 ps was then performed using a distance-dependent dielectric constant (suggested by Peter Kollman, UCSF) and followed by analysis of the resulting structures. In both simulation structures, the Ala1 nitrogen is somewhat detached from the Gla network. The TNP-Ala1/bf1 structure shows ligation of an ortho nitro-

Table VIII: Calcium–Gla Interactions (<3.0 Å)[a]

	Gla7				Gla8				Gla15				Gla17				Gla20				Gla21				Gla26				Gla27				Gla30						
cal	1	2	3	4	1	2	3	4	1	2	3	4	1	2	3	4	1	2	3	4	1	2	3	4	1	2	3	4	1	2	3	4	1	2	3	4	gla[b]	wat[c]	total[d]
1																										+	+						+		+		4	1 (0)	5 (4)
2						+		+																						+					+	+	5	2 (1)	7 (6)
3								+					+	+															+							+	5	2	7
4	+						+						+		+														+			+					6	0	7
5	x	+													x	+							s	+													4 (5)	2	6 (7)
6																		+				+	+														3	0	3
7											s	+							+	+																	4 (3)	0	4 (3)

[a] Ligation in both bf1/Ca and avg-bf1/Ca (+); ligation in bf1/Ca but not avg-bf1/Ca (x); ligation in avg-bf1/Ca but not bf1/Ca (s). Gla33 is disordered in bf1/Ca and has no metal coordination in avg-bf1/Ca. [b] gla, total number of ligatated carboxylate oxygen atoms of Gla in avg-bf1/Ca. If the number is different from that in bf1/Ca, the number in bf1/Ca is shown in parentheses. [c] wat, number of water molecules found to ligate to each calcium ion in avg-bf1/Ca. If the number is different from that in bf1/Ca, the number in bf1/Ca is shown in parentheses. [d] total, total ligation number of each calcium including ligation of Cal-4 with Asn2 in both bf1/Ca and avg-bf1/Ca.

Table IX: Close Contact to the N-Terminus of Ala1

	bf1/Ca		avg-bf1/Ca	
X	*d* (Å)	δ (deg)[a]	*d* (Å)	δ (deg)
27 OE4	3.0	−70	2.6	−48
Ca-4	3.7	−32	3.8	−9
17 OE3	2.7	−27	2.8	2
7 OE2	4.2	29	2.8	78
Ca-5	2.8	46	3.8	115
21 OE4	2.9	113	2.7	152

[a] δ is the torsion angle C(1)–Cα(1)–N(1)–X.

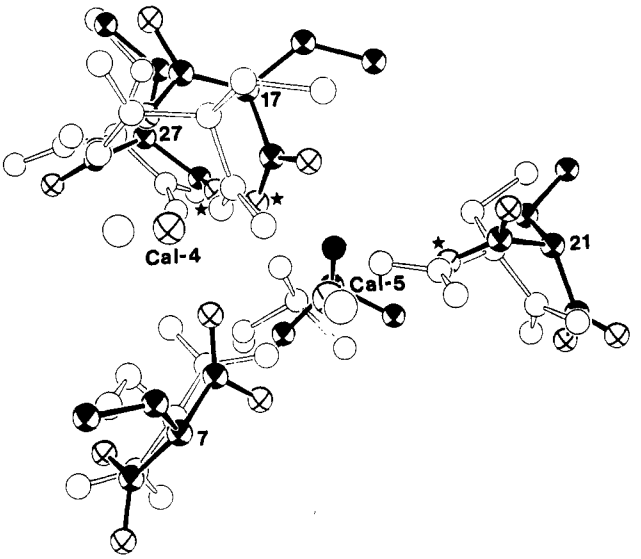

FIGURE 6: ORTEP drawing of the superposition of the amino terminus of Ala1 with neighboring residues of bf1/Ca and avg-bf1/Ca. The bf1/Ca structure is in bold; N(1) amino terminus, filled circle; carbon atoms, half-filled; Gla carboxylate oxygens, circle with cross; Gla residues numbered; asterisks designate Gla oxygens within hydrogen-bonding and/or ion-pairing distances. Ca ions (Ca-4, Ca-5), larger free standing spheres (crystallographic, with cross).

oxygen atom of TNP to Ca-5, whereas the Ace-Ala1/bf1 structure ligates the acetyl oxygen to Ca-5 in addition to having a hydrogen bond between the backbone nitrogen of Ala1 and the backbone carbonyl group of Pro22. The acetyl methyl group of the Ace-Ala1/bf1 structure is tucked into the region of the Cys18–Cys23 disulfide bond so that the turn of helix in avg-bf1/Ca (residues 15–20) is somewhat disrupted. Conversely, the TNP group is located along the surface in TNP-Ala1/bf1, giving rise to potential additional calcium-binding sites observed by an equilibrium dialysis experiment (Weber et al., 1992), while the secondary structure of residues 15–20 remains similar to avg-bf1/Ca. Since the des[Ala–Asn2]/bf1 demonstrated maintenance of membrane-binding capability (Weber et al., 1992), it is likely that N-acetylation alters the network that can be achieved by Ala1, thus precluding the necessary conformational change which is required for membrane binding.

Fluorescence. The calcium-induced intrinsic fluorescence quenching observed for bf1 is about 40% and is biphasic with a short and long time component (Nelsestuen, 1976; Pendergast & Mann, 1977; Marsh et al., 1979). On the basis of the crystal structures of apo-bf1 and bf1/Ca, it was suggested that the trans to cis isomerization of Pro54 that is observed with calcium binding might be responsible for the biphasic quenching by stabilizing interactions between the Cys18–Cys23 disulfide bridge and the conserved aromatic cluster of Phe41, Trp42, and Tyr45. The closest sulfur atom distance in the loop to an atom of Trp42 is 4.2 Å for the bf1/Ca and 5.2 Å for the avg-bf1/Ca.

The program DSSP (Kabsch & Sander, 1983) was used to evaluate the solvent-accessible surface area of the three tryptophan residues (Trp42, Trp90, Trp126) in bf1. Only Trp42 shows a substantial decrease in the solvent-accessible surface area in going from apo-bf1 (133 Å^2) to the environment containing calcium ions (64 Å^2 for bf1/Ca and 45 Å^2 for avg-bf1/Ca). Circular dichroism studies (Bloom & Mann, 1978) indicate that calcium facilitates the formation of α-helix in bf1. This agrees with the crystallographic observation that the Gla domain changes from a disordered conformation in apo-bf1 to an α-helix-rich conformation in bf1/Ca (Soriano-Garcia et al., 1992). As a consequence of the increased structural order, a highly hydrophobic environment is created around Trp42 by the side chains of five leucine residues. This is in line with suggestions that the fluorescence quenching is due to a change in hydrophobicity of the Trp42 environment in the presence of calcium. In fact, the hydrophobic interactions appear to be enhanced in avg-bf1/Ca, where the solvent-accessible surface area of Trp42 decreases by about 20 Å^2.

Calcium Sites in the Kringle Domain. Equilibrium dialysis experiments using ^{45}Ca with the kringle peptide, residues 46–156, or with fragment 1 in which all Gla residues were chemically modified (Berkowitz et al., 1992) suggests that there is at least one calcium-binding site in the kringle domain with a binding constant of 300–800 M^{-1}. However, the crystal structure of bf1/Ca did not clearly locate a calcium site in the kringle domain. In an effort to uncover a weak calcium-binding site in the kringle domain, we computed the electrostatic potential of the 46–145 protein. The nearest crystallographic water molecule to the sites with the most negative electrostatic potential was then changed to a calcium ion, and the 46–145 protein structure was minimized using a distance-dependent dielectric constant while maintaining

the positions of all other atoms in the system fixed. Two sites showed promise of calicum binding: (a) one involving the hydroxyl oxygen atoms of Ser121 (2.4 Å) and Thr123 (2.4 Å), the backbone oxygen atom of Gly124 (3.1 Å), and a nearby water molecule (2.3 Å) and (b) a site involving the backbone oxygen atoms of Val80 (2.4 Å) and Thr81 (2.3 Å), the hydroxyl oxygen atom of Ser140 (2.6 Å), and a water molecule (2.3 Å). The former site resulted from a water molecule that had the fourth lowest *B* factor (13 Å^2) of any atom in the crystal structure, whereas the latter site is near the region implicated for a calcium-binding site in the kringle domain on the basis of a study of acetylation of Ser79/Thr81 (Berkowitz et al., 1992). Both of these sites involve coordination with the side-chain hydroxyl groups of serine and threonine. Precedent for threonine coordination to calcium occurs in the crystal structure of calcium thermolysin (Holmes & Matthews, 1982), and serine coordination has been observed in the crystal structure of calcium parvalbumin (Moews & Kretsinger, 1975). Thus, the calcium ion site(s) in the kringle region could be those just described.

The structure of bf1/Ca also affords protection from acetylation of Asn101 ND2 (Welsh & Nelsestuen, 1988a). Once again, the crystallographic structure did not clearly reveal a calcium-binding site in this vicinity. However, since the carbohydrate chains attached to Asn77 and Asn101 carry several units of negative charge, it is possible that carbohydrate is responsible in protecting Asn101 from modifications in the presence of calcium. The region displays some major adjustments in going from apo-bf1 to bf1/Ca (Soriano-Garcia et al., 1992), which could also include conformational changes involving carbohydrate.

ACKNOWLEDGMENT

We have benefited substantially from a computer time grant from the North Carolina Supercomputer Center and from computer time made available at the National Cancer Institute.

REFERENCES

Berendsen, H. J. C., van Gunsteren, W. F., Swinderman, H. R. J., & Geurtsen, R. G. (1986) *Ann. N.Y. Acad. Sci. 482*, 269–286.

Berkowitz, P., Huh, N.-W., Brostrom, K. E., Panek, M. G., Weber, D. J., Tulinsky, A., Pedersen, L. G., & Hiskey, R. G. (1992) *J. Biol. Chem. 267*, 4570–4576.

Bloom, J. W., & Mann, K. G. (1978) *Biochemistry 17*, 4430–4438.

Charifson, P. S., Darden, T., Tulinsky, A., Hughey, J., Hiskey, R. G., & Pedersen, L. (1991) *Proc. Natl. Acad. Sci. U.S.A. 88*, 424–428.

Darden, T., Johnson, P., & Smith, H (1991) *J. Mol. Graphics 9*, 18–23.

Deerfield, D. W. (1991) Program DIST, Pittsburgh Supercomputer Center, Pittsburgh, PA.

Deerfield, D. W., Olson, D. L., Berkowitz, P., Koehler, K. A., Pedersen, L. G., & Hiskey, R. G. (1987) *Biochem. Biophys. Res. Commun. 144*, 520–527.

Holmes, M. A., & Matthews, B. W. (1982) *J. Mol. Biol. 160*, 623–639.

Jorgensen, W. L., Chandrasekhar, J., Madura, J. D., Impey, R. W., & Klein, M. L. (1983) *J. Chem. Phys. 79*, 926–935.

Kabsch, W. (1986) *Acta. Crystallogr. A32*, 922–933.

Kabsch, W., & Sander, C. (1983) *Biopolymers 22*, 2577–2637.

Lundblad, R. (1988) *Biochem. Biophys. Res. Commun. 157*, 295–300.

Mann, K. G. (1987) *Trends Biochem. Sci. 12*, 229–233.

Marsh, H. C., Scott, M. E., Hiskey, R. G., & Koehler, K. A. (1979) *Biochem. J. 183*, 513–517.

Maynard, A. T., Eastman, E. A., Darden, T., Deerfield, D. W., Hiskey, R. G., & Pedersen, L. G. (1988) *Int. J. Pept. Protein Res. 31*, 137–149.

Moews, P. C. & Kretsinger, R. H. (1975) *J. Mol. Biol. 91*, 201–226.

Mulichak, A. M., Tulinsky, A., & Ravichandran, K. G. (1991) *Biochemistry 30*, 10576–10588.

Nelsestuen, G. L. (1986) *J. Biol. Chem. 251*, 5648–5656.

Olson, R. E. (1984) *Annu. Rev. Nutr. 4*, 281–337.

Olsson, G., Andersen, L., Lindquist, O., Sjolin, L., Magnusson, S., Peterssen, T. E., & Sottrup-Jensen, L. (1982) *FEBS Lett. 145*, 317–322.

Park, C. H., & Tulinsky, A. (1986) *Biochemistry 25*, 3977–3982.

Pendergast, F. G., & Mann, K. G. (1977) *J. Biol. Chem. 252*, 840–850.

Ryckaert, J. P., Ciccotti, G., & Berendsen, H. C. (1977) *J. Comput. Phys. 23*, 327–341.

Seshadri, T. P., Tulinsky, A., Skrzypczak-Jankun, E., & Park, C. H. (1991) *J. Mol. Biol. 220*, 481–494.

Soriano-Garcia, M., Park, C. H., Tulinsky, A., Ravichandran, K. G., & Skrzypczak-Jankun, E. (1989) *Biochemistry 28*, 6805–6810.

Soriano-Garcia, M., Padmanabhan, K., deVos, A. M., & Tulinsky, A. (1992) *Biochemistry 31*, 2554–2566.

Suttie, J. W. (1988) *Biofactors 1*, 55–60.

Suttie, J. W., & Jackson, C. M. (1977) *Physiol. Rev. 57*, 1–70.

Tulinsky, A. (1991) *Thromb. Haemostasis 66*, 16–31.

Tulinsky, A., Park, C. H., & Skrzypczak-Jankun, E. (1988) *J. Mol. Biol. 203*, 885–901.

Weber, D., Berkowitz, P., Panek, M. G., Huh, N.-W., Pedersen, L. G., & Hiskey, R. G. (1992) *J. Biol. Chem. 267*, 4564–4569.

Weiner, S. J., Kollman, P. A., Case, D. A., Singh, U. C., Chio, C., Alagona, C., Profeta, S., Jr., & Weiner, P. (1984) *J. Am. Chem. Soc. 106*, 765–784.

Weiner, S. J., Kollman, P. A., Nguyen, D. T., & Case, D. A. (1986) *J. Comput. Chem. 7*, 230–252.

Welsch, D. J., & Nelsestuen, G. L. (1988a) *Biochemistry 27*, 4939–4945.

Welsch, D. J., & Nelsestuen, L. (1988b) *Biochemistry 27*, 4946–4952.

Wu, T.-P., Padmanabhan, K., Tulinsky, A., & Mulichak, A. M. (1991) *Biochemistry 30*, 10589–10594.

Registry No. Gla, 53445-96-8.